Cardiovascular Informatics: A Perspective on Promises and Challenges of IVUS Data Analysis

Ioannis A. Kakadiaris and E. Gerardo Mendizabal Ruiz

Abstract Intravascular ultrasound (IVUS) is a catheter-based medical imaging modality that is capable of providing cross-sectional images of the interior of blood vessels. A comprehensive analysis of the IVUS data allows collecting information about the morphology and structure of the vessel and the atherosclerotic plaque, if present. Atherosclerotic plaque formation is considered to be a part of an inflammatory process. Recent evidence has suggested that the presence and proliferation of vasa vasorum (VV) in the plaque is correlated with the increase of plaque inflammation and the processes which lead to its destabilization. Hence, the detection and measurement of VV in plaque has the potential to enable the development of an index of plaque vulnerability. In this paper, we review the research at the Computational Biomedicine Lab towards the development of a complete pipeline for the detection and quantification of extra-luminal blood detection from IVUS data which may be an indication of the existence of VV.

Mathematics Subject Classification (2010): Primary 68U99, Secondary 68U01

I.A. Kakadiaris (✉)
Computational Biomedicine Lab, Departments of Computer Science, Electrical and Computer Engineering, and Biomedical Engineering, University of Houston, Houston, TX 77204, USA
e-mail: ioannisk@uh.edu

E.G. Mendizabal Ruiz
Computational Biomedicine Lab, Department of Computer Science, University of Houston, Houston, TX 77204, USA
e-mail: gerardomendizabal@gmail.com

P.M. Pardalos et al. (eds.), *Optimization and Data Analysis in Biomedical Informatics*, Fields Institute Communications 63, DOI 10.1007/978-1-4614-4133-5_6,

1 Introduction

Complications attributed to cardiovascular disease (CVD) constitute a major cause of death worldwide. One of the primary causes of CVD is coronary artery disease (CAD), which is a narrowing of the small blood vessels that supply blood and oxygen to the heart. CAD is caused by a condition called atherosclerosis, which occurs due to the accumulation of plaque on the inner walls of the arteries. The progression of this condition may lead to inflammation of the coronary arteries and the consequent obstruction of blood flow to the heart. But more critically, the sudden rupture of a plaque (i.e., thrombotic-related complications) may lead to a stenotic condition in which the blood supply is entirely cutoff from a region of the heart, resulting in death. In this context, the field of cardiology has introduced the term "vulnerable plaque" in reference to the plaques with a high likelihood of rupture, thrombotic complications, and the consequent rapid progression to stenosis [26–29]. Vasa vasorum ("vessels of the vessels", VV) is a network of microvessels that penetrates and "feeds" the vessel wall [13]. Recent evidence has suggested that the presence and proliferation (i.e., increase in density) of VV in the plaque is correlated to an increase in plaque inflammation and the processes which lead to its destabilization [1, 4, 7, 10, 12, 21, 22]. Hence, it is believed that the detection and measurement of VV in plaque and the detection of leakage of blood within atherosclerotic plaques have the potential to enable the development of an index of plaque vulnerability [3, 15].

Intravascular ultrasound (IVUS) is a catheter-based medical imaging technique that is capable of providing cross-sectional images of the interior of blood vessels and is currently the gold-standard technique for assessing the morphology of blood vessels and atherosclerotic plaques in vivo [42]. An IVUS system consists of a catheter with a miniaturized ultrasound probe attached to its tip. The ultrasound probe transmits ultrasound pulses and receives an acoustic radio frequency (RF) echo signal (i.e., A-line) at a discrete set of angles. A B-mode IVUS image is obtained by computing the positive envelopes of each A-line (Fig. 1a). The B-mode signals are compressed, stacked along the angular direction, and mapped into an 8-bit gray scale to form an image known as the polar B-mode image (Fig. 1b). To provide a more familiar representation of the data (i.e., one that resembles the interior of a vessel), the polar B-mode image is geometrically transformed to obtain a disc-shaped image known as the Cartesian B-mode image (Fig. 1c). Similar to other ultrasound modalities, IVUS may be used in combination with contrast agents [47] delivered as microbubbles which are of a size similar to red blood cells (diameter: 1–10 μm). These microbubbles resonate in response to the pressure changes induced by the ultrasound wave and are highly echogenic when compared to normal body tissues. As a result, they appear bright in the B-mode ultrasound images, and can hence be used as tracers of blood flow [3, 11].

Since VV may be found in the atherosclerotic plaque and/or the wall of the vessel (i.e., extra-luminal regions), the problem of VV detection can be posed as the detection of extra-luminal blood perfusion. In this paper, we present our studies

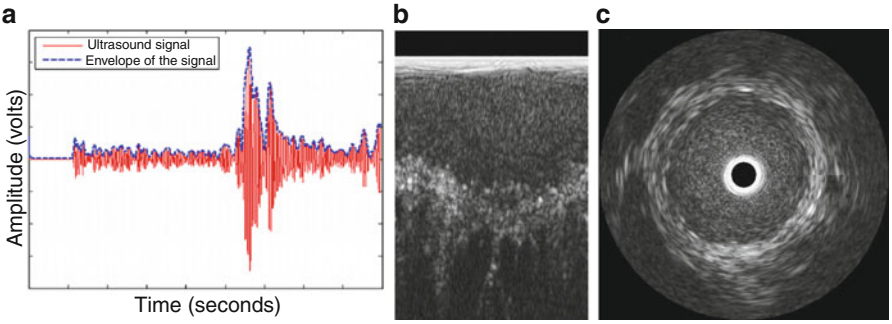

Fig. 1 Depiction of (**a**) A-line signal and its envelope, examples of the B-mode (**b**) polar, and (**c**) Cartesian IVUS images

towards the detection and quantification of extra-luminal blood perfusion, which can be categorized as: (1) methods for the detection of the lumen contour, and (2) methods for the detection of blood perfusion. The rest of this paper is organized as follows: In Sect. 2, we present a brief summary of methods that have been proposed for the analysis of IVUS data. In Sect. 3, we describe the methods for solving the extra-luminal blood detection problem. The results obtained with the proposed methods are presented in Sect. 4, and in Sect. 5, we present our conclusions.

2 Previous Work

IVUS Segmentation: Segmentation of IVUS data refers to the delineation of the lumen/intima and media/adventitia borders. This procedure is useful for studying atherosclerosis diseases, since it provides an assessment of the vascular wall, and also provides information on the nature of atherosclerotic lesions and information about the shape and size of the plaque. Automatic methods for IVUS segmentation are required as there are a large number of frames in an IVUS sequence, thereby making manual segmentation of a sequence infeasible (within a reasonable time). Some of the most recent approaches for automatic IVUS segmentation include a shape-driven method for lumen and media-adventitia segmentation introduced by Unal et al. [45] that uses Principal Component Analysis (PCA) to create a shape space from previously segmented frames. Segmentation is accomplished by the minimization of an energy function using nonparametric probability densities with global measurements. Taki et al. [44] proposed a method that involved preprocessing of the IVUS images, and the posterior deformation of geometric and parametric models using edge information. Downe et al. [6] introduced a method where PCA was first used for pre-processing. Active contour models were then used to provide an initial segmentation for a 3D graph search method. Multilevel discrete wavelet frame decomposition was used by Papadogiorgaki et al. [38] to generate

texture information that was used along with the intensity information for contour initialization. Low pass filters and radial basis functions were then used to refine the contour. Similarly, Katouzian et al. [17] proposed a method where texture information was extracted using a discrete wavelet packet transform. The pixels of the IVUS image were then classified as lumen or non-lumen using k-means clustering. Finally, the contour was parameterized using a spline curve. Ciompi et al. [5] presented a method in which segmentation was tackled as a classification problem and solved using an error correcting output code technique. In this work, contextual information was exploited by means of conditional random fields computed from training data. The most common limitation of the segmentation methods discussed above is the lack of robustness with respect to noise, IVUS image variability, and the different artifacts that can appear in an IVUS image.

Tissue Characterization: Tissue characterization from IVUS data involves a definition of composition (e.g., fibrous, calcified, or lipid) of the atherosclerotic plaque based on the changes that occur to the sound waves as they interact with the different tissues. A common approach for characterization is to compute different texture features from the gray-level IVUS B-mode representation (e.g., co-occurrence matrix, laws features, Gabor filters). These features are used to train a classification model which is then used to predict the tissue classes on new data [2, 16, 41, 50]. The most successful approaches for the characterization of plaque are based on the analysis of the IVUS-RF signal data instead of the B-mode data. Nair et al. [30, 31] proposed a method known as "virtual histology" (IVUS-VH) that is based on the power spectral analysis (intercept, slope, mid-band fit, and minimum and maximum powers and their corresponding frequencies) of the IVUS-RF signals combined with classification trees. High accuracy (>85%) was reported for differentiating fibrous, fibrofatty, calcified, and necrotic regions. In addition, Rodriguez-Granillo et al. [40] and Nasu et al. [32], presented the results of *in-vivo* studies using the above method and reported a high correlation with the corresponding histology. Kawasaki et al. [18, 19] proposed a method for tissue classification using the integrated backscatter (IB), which is a parameter derived from the RF signal that is used to divide the tissue into five categories: thrombus, intimal hyperplasia or lipid core, fibrous tissue, mixed lesions and calcification. This method has demonstrated high sensitivity and specificity for characterizing calcification (100%, 99%), fibrosis (94%, 84%), and lipid pool (84%, 97%) [20]. O'Malley et al. [36] presented a study of the feasibility of blood characterization on IVUS data using features intended to quantify speckle and features based on frequency-domain measures of high-frequency signal using one-class support vector machines on the RF raw signal, the signal envelope and the log-compressed signal envelope. The feasibility of using wavelet analysis of the RF amplitude for plaque characterization [16,41] and blood classification [17] was also studied. However, the majority of these methods are not suitable for blood detection since they focus on the characterization of the atherosclerotic plaque components. Also, the methods that have been proposed for blood detection are not capable of detecting small extra-luminal blood perfusion.

Perfusion Detection: O'Malley et al. [14, 34, 37, 46, 48, 49] proposed a protocol and an automatic algorithm (Analysis of Contrast Enhanced Sequences, ACES) for the quantification and visualization of VV in contrast-enhanced IVUS image sequences. That method relies on the detection of local echogenicity changes in stationary IVUS sequences caused by microbubble perfusion into the vessel wall. The proposed protocol consisted of acquiring images from a suspect plaque while a bolus injection of contrast agent was performed. The detection of extra-luminal blood was performed offline and involved two steps: (1) image stabilization [33,35] (i.e., image-based gating and registration), and (2) detection of enhancement, which was based on a comparison of the stabilized pre-contrast baseline images and the post-injection images. As a result, any change that occurred due to contrast enhancement would be reflected as a positive difference in the intensities. The enhancement was quantified and certain statistics were computed. The main limitation of this method is that it requires the alignment of frames which is very difficult to achieve even with the proposed stabilization methods. Goertz et al. [8, 9] proposed a solution for perfusion detection based on the detection of the harmonic and sub-harmonic response of the contrast microbubbles. The limitation of these methods is the requirement of a specially designed, non-commercial IVUS system.

3 Methods

Our proposed framework for the detection and quantification of extra-luminal blood perfusion consists of two steps: (1) detection of the luminal border, and (2) detection of extra-luminal perfusion. In the following subsections, we review the proposed methods for the above mentioned tasks.

3.1 Lumen Segmentation

Image-Based Segmentation: In this method, we employ the B-mode polar IVUS image representation for the segmentation of the lumen. This choice makes the computations much simpler due to the 1D appearance of the lumen contour. We define a function $f(\theta, c)$ as the curve that represents the change of interface between the lumen and the vessel wall. Since we know that the shape of the vessel's wall is essentially smooth, and that a polar B-mode IVUS image is periodic with respect to the horizontal axis, we parameterize the function that represents the lumen contour using Fourier series. The lumen segmentation problem consists of finding the optimum parameters c^* such that the curve $f(\theta, c^*)$ corresponds to the interface between the lumen and the vessel wall. This is accomplished by minimizing a cost function formulated using a Bayesian approach in which we incorporate *a priori*

information about the regions of lumen and non-lumen based on the prediction of a support vector machine (SVM) classifier, trained with samples from the lumen and wall regions provided by the user [25].

RF-Based Segmentation: The use of B-mode images for IVUS data analysis poses a limitation due to the loss of information resulting from the B-mode conversion and the fact that the appearance of the B-mode images depends on the characteristics of the IVUS system which varies between systems, and on the visualization parameters (e.g., time gain compensation, compression, brightness, contrast) that are subjectively adjusted by the interventionist. To overcome this limitation, one has to work directly with the raw IVUS RF signal as it is not affected by the transformation or visualization parameters. Based on this observation, we developed a method for the segmentation of the lumen contour using the IVUS RF signal based on a physics-based model of the interaction of the sound waves with the tissues of the vessel [23].

When an incident sound wave interacts with an object, a fraction of its power will be reflected and a fraction will be absorbed by the object. When the wavelength of the incident wave is smaller in comparison with the size of the object, the reflection will occur in many directions (i.e., scattering). The power scattered by each scatterer object in the direction opposite to the direction of the incident wave is referred to as the *differential backscattering cross section* (DBC) [43]. If we consider that the wavelength of the IVUS impulse signal is large in comparison with the structures in the vessel, we can model the received IVUS RF signal, $\hat{S}_k(t)$, for each transducer's angular position (i.e., A-line) by representing the structures in the vessel as a finite set of point scatterers with an associated DBC coefficient. Our RF-based segmentation method consists of two steps: (1) a calibration step in which we estimate the parameters of the model using the RF signal of a manually segmented frame from the sequence to be segmented by employing an inverse problem approach, and (2) the detection of lumen contour by locating the change of interface for each A-line, by minimizing the cost function that employs the RF signal and the calibrated scattering model. Both the steps are based on the following assumptions: (1) there are only two types of tissue or layers within the vessel: lumen (blood) and wall; (2) the DBC coefficient of blood is different from the DBC coefficient of wall; (3) scatterers within the same layer will have the same DBC; (4) the attenuation coefficient is constant along the radial direction; and (5) the real IVUS signal can be approximated using a stochastic minimization process that employs random samples of the scatterers' positions. Since the lumen interface for each angle is recovered independently, it is very likely that the resulting curve is not smooth or periodic. Moreover, due to noise or artifacts, it is possible that our method obtains an incorrect result in one or more angles. Therefore, we introduce a post-processing step in which the lumen contour is constrained to a smooth periodical curve using Fourier series parameterization by applying a spectral smoothing method [39].

3.2 Perfusion Detection

Contrast Agent Detection: We investigated the feasibility of detecting the contrast agent on IVUS sequences by characterizing the RF IVUS signal using two contrast detection classifiers (CDC) based on one-class cost-sensitive learning [24]. In the first contrast detection classifier (CDC_1), we build a model for the detection of contrast agent using samples of the contrast agent present in the lumen during the microbubble injection. In the second contrast detection classifier (CDC_2), we detect the contrast agent as a change from baseline IVUS (i.e., lumen, intima, media and adventitia signals acquired from frames prior to the bolus injection). The primary advantage of these methods is that, by using the RF IVUS data, we do not lose information contained in the frequency of the signal. The second advantage is that, by using one-class learning, we do not need to provide "background" samples for building the classifiers. This is particularly important to this study because, although samples for contrast agent in lumen can be acquired by manual annotations from an expert, the background can consist of a wide variety of other imaged tissues. Thus, obtaining samples for the other tissues may be difficult and labor-intensive.

The features that characterize contrast agent and the baseline IVUS are defined for a 3-D window of size $r \times \theta \times t$. These features are computed by stacking consecutive frames over time, and obtaining a 3D IVUS signal volume $S(R, \Theta, T)$, where R indicates the radial distance from the transducer, Θ is the angle with respect to an arbitrary origin, and T is the time elapsed since the start of the recording (i.e., frame number). We study the feasibility of characterizing the contrast agent's signal using two types of features: features based on frequency-domain spectral characterization (as proposed by O'Malley et al. [36]) and features based on 2-level 2D discrete wavelet decomposition.

Blood Detection: We assumed that that the signal of a partition corresponding to certain tissue can be characterized by the DBC coefficient that generates that signal. We employ the scattering model for computing the DBC corresponding to a partition of the RF-signal of an A-line. Our objective is to find the DBC value that minimizes the difference between the root mean square power (RMS) of the signal of a given partition and the RMS power of the signal generated by our model. We divide the real and modeled signal of each angle θ into N_P non-overlapping partitions of the same size $\triangle P$. The initial and final times (α_p and β_p, respectively) for each partition $P_{\theta,p}$ are computed such that $\triangle P = (\beta_p - \alpha_p) \forall\, p$, and the RMS of each partition of the real and modeled signals ($R_{\theta,p}$ and $\hat{R}_{\theta,p}$, respectively) are computed. In order to find the DBC value that generates the signal in each partition we find the value $\tau_{\theta,p}$ such that the quadratic error E between the RMS power of the real and modeled signals for the partition $P_{\theta,p}$ is minimal. The RMS power of the modeled signal depends on the spatial position arrangement of the scatterers. Since these positions are unknown, we employ the Monte-Carlo approach on which we perform several computations based on several random scatterer's positions. The problem of finding the DBC for each partition is formulated as a system of linear equations and solved very efficiently. Since we consider that there may exist a certain degree of overlap

between the ultrasound beams of consecutive angles due to the angular divergence of the beam, we introduce a regularization term that embodies our assumptions about the variation of the DBC value of each partition and its neighbors.

4 Results

Image-Based Segmentation: The first 50 frames from nine sequences of 20 MHz data (i.e., 450 frames in total) and nine sequences of 40 MHz data (i.e., 405 frames in total) were used for comparing the results of the automatic segmentation method with the manual segmentation from two expert observers. In order to evaluate the performance of the method, we computed the Dice similarity coefficient (degree of overlap between segmentation) along with linear regression and Bland-Altman analysis (comparison of lumen areas). The results indicated a high Dice similarity coefficient for the 20 MHz and 40 MHz datasets (0.95 and 0.93, respectively). The linear regression plots exhibited a high correlation between the measured areas obtained by the automatic and the manual segmentations. In addition, Bland-Altman analysis of the data indicated that the performances of the automatic method and the human observers are comparable. Figure 2 depicts examples of the segmentation results obtained with the proposed method.

RF-Based Segmentation: We evaluated the performance of the proposed method using the RF data from 490 frames corresponding to fourteen 40 MHz pullback IVUS sequences obtained from rabbit aortas and various coronary arteries of swine, and compared the results with those obtained through the the manual segmentation by expert observers. The average Dice similarity was 0.96 while the mean bias and the linear regression also showed that the performance of the automatic method and the human observers is comparable. Figure 3 depicts examples of the segmentation results obtained with the proposed method.

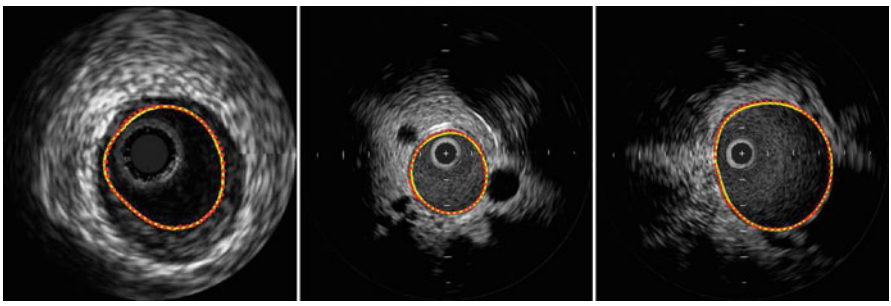

Fig. 2 Examples of automatic image-based segmentation results. The *solid* and *dotted lines* correspond to the automatic and manual segmentation, respectively

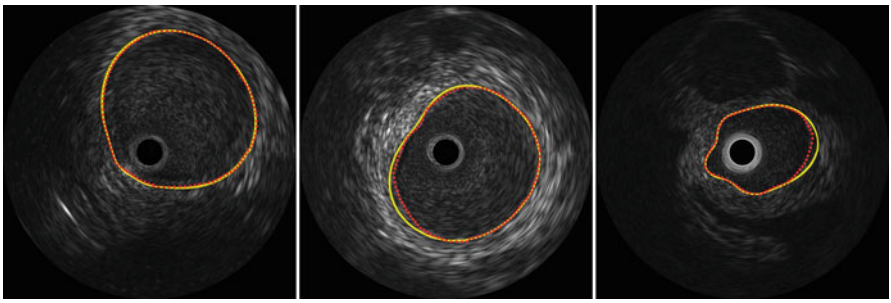

Fig. 3 Examples of automatic RF-based automatic segmentation results. The *solid* and *dotted lines* correspond to the automatic and manual segmentation, respectively

Contrast Agent Detection: Samples from two contrast-enhanced IVUS sequences obtained from swine were used to evaluate the feasibility of the proposed method. The best performance, for both CDCs and the two types of features, was obtained when using a window of size $r = 255$, $\theta = 7$, and $t = 13$. For the frequency-domain features, the best average performance for contrast detection (CD) and blood rejection (BR) with CDC_1 is CD = 96.61% and BR = 95.67%. With CDC_2 BD = 96.79% and CR = 94.24%. The best performance for wavelet-based features with CDC_1 is CD = 96.79% and BR = 94.13%. With CDC_2 BD = 98.51% and CR = 96.94%. Figure 4 depicts examples of the classification results obtained with the proposed method.

Blood Detection Results: Experiments were performed using real IVUS RF data from six 40 MHz pullback sequences corresponding to different arteries from rabbits and swines. For each sequence we compared the recovered DBC values for blood and non-blood samples acquired from manual annotations provided by an expert. The recovered DBC values for blood and non-blood were very similar for sequences acquired using the same IVUS system and from the same species. Additionally, as a preliminary blood detection experiment, we used our method to recover the DBC values from the IVUS RF data of a frame corresponding to a 40 MHz IVUS pullback from swine, for which histological information is available (Fig. 5a). We normalized the resulting DBC values for each pixel of the image and depicted the frame using a color palette (Fig. 5c). The regions of the resulting image that correspond to vascularization were manually annotated according to the criterion that a vessel should contain a region of DBC values corresponding to blood surrounded by DBC values corresponding to non-blood. These results are very encouraging as they provide preliminary evidence that our method could be used for computation of a feature that leads to automatic blood detection.

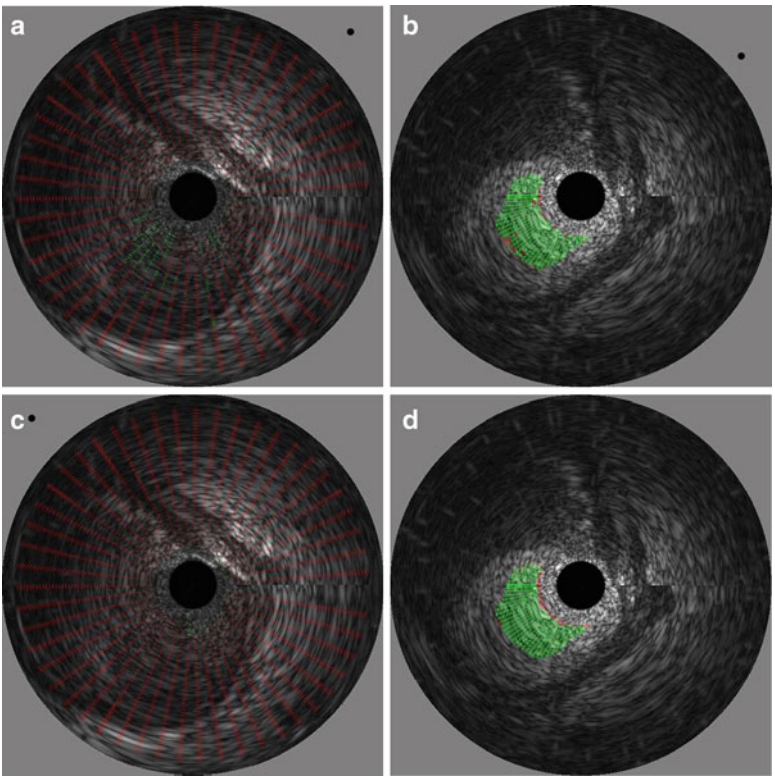

Fig. 4 Examples of classification results for CDC_1 using the frequency-domain-based (**a**,**b**) and wavelet-based features (**c**,**d**) in an IVUS frame before injection (**a**,**c**) and during the injection (**b**,**d**). The *green color* indicates the pixels classified as contrast agent and the *red color* indicates the pixels classified as non-contrast agent

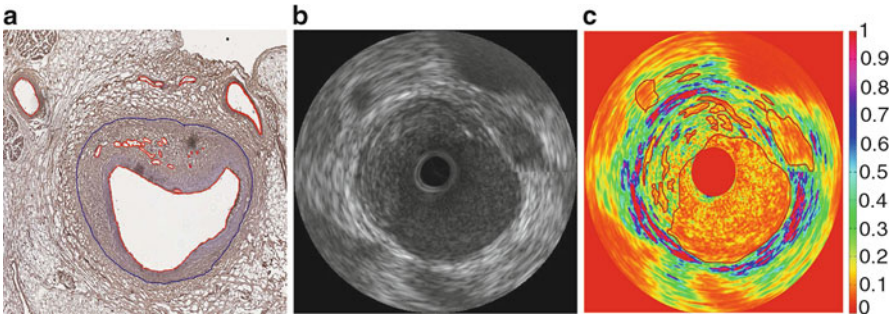

Fig. 5 Annotation of vasculature on (**a**) histological sample, (**b**) its corresponding B-mode Cartesian image, and (**c**) recovered DBC values using a color palette with annotation of blood regions

5 Conclusion

We have reviewed the proposed methods towards the development of a complete framework for the automatic detection of extra-luminal blood. The initial results of this study are very encouraging and we believe that further research in this direction will lead to the development of a fast and reliable method for VV detection and quantification.

Acknowledgements This work was supported in part by the Eckhard Pfeiffer Endowed Fund and by NSF grants IIS-0431144, CNS-0521527 and DMS-0915242. The second author was supported in part by CONACYT. Any opinions, findings, conclusions or recommendations expressed in this material are the authors' and may not reflect the views of the sponsors.

References

1. K.R. Balakrishnan, S. Kuruvilla, Role of inflammation in atherosclerosis: Immunohistochemical and electron microscopic images of a coronary endarterectomy specimen. Circulation **113**, e41–e43 (2006)
2. K. Caballero, J. Barajas, O. Pujol, J. Mauri, P. Radeva. In-Vivo IVUS Tissue Classification a Comparison Between Normalized Image Reconstruction and RF Signals Analysis. Proceedings of 11^{th} Iberoamerican Congress on Pattern Recognition, Cancun, Mexico, pp. 137–146 (2006)
3. S. Carlier, I. Kakadiaris, N. Dib, M. Vavuranakis, C. Stephanadis, S. O'Malley, C. Hartley, R. Metcalfe, R. Mehran, E. Falk, K. Gul, M. Naghavi, Vasa vasorum imaging: A new window to the clinical detection of vulnerable atherosclerotic plaques. Curr. Atherosclerosis Rep. **7**(2), 164–169 (2005)
4. F. Chen, P. Eriksson, T. Kimura, I. Herzfeld, G. Valen, Apoptosis and angiogenesis are induced in the unstable coronary atherosclerotic plaque. Coron. Artery Dis. **16**(3), 191–197 (2005)
5. F. Ciompi, O. Pujol, E. Fernandez-Nofrerias, J. Mauri, P. Radeva, ECOC Random Fields for Lumen Segmentation in Radial Artery IVUS Sequences. Proceedings of 12^{th} International Conference on Medical Image Computing and Computer Assisted Intervention, London, UK, pp. 869–876, 20–24 September 2009
6. R. Downe, A. Wahle, T. Kovarnik, H. Skalicka, J. Lopez, J. Horak, M. Sonka. Segmentation of Intravascular Ultrasound Images Using Graph Search and a Novel Cost Function. Proceedings of 2^{nd} MICCAI Workshop on Computer Vision for Intravascular and Intracardiac Imaging, New York, NY, pp. 71–79, 10 September 2008
7. M. Fleiner, M. Kummer, M. Mirlacher, G. Sauter, G. Cathomas, R. Krapf, B.C. Biedermann, Arterial neovascularization and inflammation in vulnerable patients. Circulation **110**(18), 2843–2850 (2004)
8. D.E. Goertz, M.E. Frijlink, N. de Jong, A.F. van der Steen, Nonlinear intravascular ultrasound contrast imaging. Ultrasound Med. Biol. **32**(4), 491–502 (2006)
9. D.E. Goertz, M.E. Frijlink, D. Tempel, V. Bhagwandas, A. Gisolf, R. Krams, N. de Jong, A.F.W. van der Steen, Subharmonic contrast intravascular ultrasound for vasa vasorum imaging. Ultrasound Med. Biol. **33**(12), 1859–1872 (2007)
10. M. Gossl, N. Malyar, M. Rosol, P. Beighley, E. Ritman, Impact of coronary vasa vasorum functional structure on coronary vessel wall perfusion distribution. Am. J. Physiol. Heart Circ. Physiol. **285**(5), H2019–H2026 (2003)

11. J. Granada, S. Feinstein, Imaging of the vasa vasorum. Nat. Rev. Cardiol. **5**(2s), S18–S25 (2008)
12. M. Hayden, S. Tyagi, Vasa vasorum in plaque angiogenesis, metabolic syndrome, type 2 diabetes mellitus, and atherosclerosis: A malignant transformation. Cardiovasc. Diabetol. **3**(1), 1–16, 2004
13. D.D. Heistad, M.L. Marcus, Role of vasa vasorum in nourishment of the aorta. Blood Ves. **16**, 225–238 (1979)
14. I. Kakadiaris, S. O'Malley, M. Vavuranakis, S. Carlier, R. Metcalfe, C. Hartley, E. Falk, M. Naghavi, Signal processing approaches to risk assessment in coronary artery disease. IEEE Signal Process. Mag. **23**(6), 59–62 (2006)
15. I. Kakadiaris, U. Kurkure, E. Mendizabal-Ruiz, M. Naghavi, Towards Cardiovascular Risk Stratification Using Imaging Data. Proceedings of 31^{st} International Conference of the IEEE Engineering in Medicine and Biology Society, Minneapolis, MN, pp. 1918–1921, 2–6 September 2009
16. A. Katouzian, B. Baseri, E.E. Konofagou, A.F. Laine, An Alternative Approach to Spectrum-Based Atherosclerotic Plaque Characterization Techniques Using Intravascular Ultrasound (IVUS) Backscattered Signals. Proceedings of 2^{nd} MICCAI Workshop on Computer Vision for Intravascular and Intracardiac Imaging, New York, NY, 2008
17. A. Katouzian, B. Baseri, E. Konofagou, A. Laine, Automatic Detection of Blood Versus Non-Blood Regions on Intravascular Ultrasound (IVUS) Images Using Wavelet Packet Signatures. Proceedings of SPIE Medical Imaging 2008: Ultrasonic Imaging and Signal Processing, San Diego, CA, 16–21 February 2008
18. M. Kawasaki, H. Takatsu, T. Noda, Y. Ito, A. Kunishima, M. Arai, K. Nishigaki, G. Takemura, N. Morita, S. Minatoguchi, H. Fujiwara, Noninvasive quantitative tissue characterization and two-dimensional color-coded map of human atherosclerotic lesions using ultrasound integrated backscatter: Comparison between histology and integrated backscatter images. J. Am. Coll. Cardiol. **38**(2), 486–492 (2001)
19. M. Kawasaki, H. Takatsu, T. Noda, K. Sano, Y. Ito, K. Hayakawa, K. Tsuchiya, M. Arai, K. Nishigaki, G. Takemura, S. Minatoguchi, T. Fujiwara, H. Fujiwara, In vivo quantitative tissue characterization of human coronary arterial plaques by use of integrated backscatter intravascular ultrasound and comparison with angioscopic findings. Circulation **105**, 2487–2492 (2002)
20. M. Kawasaki, B. Bouma, J. Bressner, S. Houser, S. Nadkarni, B. MacNeill, I. Jang, H. Fujiwara, G. Tearney, Diagnostic accuracy of optical coherence tomography and integrated backscatter intravascular ultrasound images for tissue characterization of human coronary plaques. J. Am. Coll. Cardiol. **48**(1), 81–88 (2006)
21. F. Kolodgie, H. Gold, A. Burke, D. Fowler, H. Kruth, D. Weber, A. Farb, L. Guerrero, M. Hayase, R. Kutys, J. Narula, A. Finn, R. Virmani, Intraplaque hemorrhage and progression of coronary atheroma. New Engl. J. Med. **349**(24), 2316–2325 (2003)
22. A.C. Langheinrich, A. Michniewicz, D.G. Sedding, G. Walker, P.E. Beighley, W.S. Rau, R.M. Bohle, E.L. Ritman, Correlation of vasa vasorum neovascularization and plaque progression in aortas of apolipoprotein E(-/-)/low-density lipoprotein(-/-) double knockout mice. Arterioscler. Thromb. Vasc. Biol. **26**(2), 347–352 (2006)
23. E. Mendizabal-Ruiz, G. Biros, I.A. Kakadiaris, An Inverse Scattering Algorithm for the Segmentation of the Luminal Border on Intravascular Ultrasound Data. Proceedings of 12^{th} International Conference on Medical Image Computing and Computer Assisted Intervention, London, UK, pp. 885–892, 20–24 September 2009
24. E. Mendizabal-Ruiz, I. Kakadiaris, One-Class Acoustic Characterization Applied to Contrast Agent Detection in IVUS. Proceedings of International Workshop on Computer Vision for Intravascular and Intracardiac Imaging, New York, NY, 10 September 2008
25. E. Mendizabal-Ruiz, M. Rivera, I. Kakadiaris, A Probabilistic Segmentation Method for the Identification of Luminal Borders in Intravascular Ultrasound Images. Proceedings of IEEE Computer Society Conference on Computer Vision and Pattern Recognition, Anchorage, AK, pp. 1–8, 24–26 June 2008

26. A.K. Mitra, A.S. Dhume, D.K. Agrawal, "Vulnerable plaques" – ticking of the time bomb. Can. J. Physiol. Pharmacol. **82**(10), 860–871 (2004)
27. M. Naghavi, P. Libby, E. Falk, S. Casscells, S. Litovsky, J. Rumberger, J. Badimon, C. Stefanadis, P. Moreno, G. Pasterkamp, Z. Fayad, P. Stone, S. Waxman, P. Raggi, M. Madjid, A. Zarrabi, A. Burke, C. Yuan, P. Fitzgerald, D. Siscovick, C. de Korte, M. Aikawa, K. Airaksinen, G. Assmann, C. Becker, J. Chesebro, A. Farb, Z. Galis, C. Jackson, I. Jang, W. Koenig, R. Lodder, K. March, J. Demirovic, M. Navab, S. Priori, M. Rekhter, R. Bahr, S. Grundy, R. Mehran, A. Colombo, E. Boerwinkle, C. Ballantyne, J. Insull, W., R. Schwartz, R. Vogel, P. Serruys, G. Hansson, D. Faxon, S. Kaul, H. Drexler, P. Greenland, J. Muller, R. Virmani, P. Ridker, D. Zipes, P. Shah, J. Willerson, From vulnerable plaque to vulnerable patient: A call for new definitions and risk assessment strategies: Part I. Circulation **108**(14), 1664–1672 (2003)
28. M. Naghavi, P. Libby, E. Falk, S. Casscells, S. Litovsky, J. Rumberger, J. Badimon, C. Stefanadis, P. Moreno, G. Pasterkamp, Z. Fayad, P. Stone, S. Waxman, P. Raggi, M. Madjid, A. Zarrabi, A. Burke, C. Yuan, P. Fitzgerald, D. Siscovick, C. de Korte, M. Aikawa, K. Airaksinen, G. Assmann, C. Becker, J. Chesebro, A. Farb, Z. Galis, C. Jackson, I. Jang, W. Koenig, R. Lodder, K. March, J. Demirovic, M. Navab, S. Priori, M. Rekhter, R. Bahr, S. Grundy, R. Mehran, A. Colombo, E. Boerwinkle, C. Ballantyne, W. Insull, R. Schwartz, R. Vogel, P. Serruys, G. Hansson, D. Faxon, S. Kaul, H. Drexler, P. Greenland, J. Muller, R. Virmani, P. Ridker, D. Zipes, P. Shah, J. Willerson, From vulnerable plaque to vulnerable patient: A call for new definitions and risk assessment strategies: Part II. Circulation **108**(15), 1772–1778 (2003)
29. M. Naghavi, E. Falk, H. Hecht, M. Jamieson, S. Kaul, D. Berman, Z. Fayad, M. Budoff, J. Rumberger, T. Naqvi, L. Shaw, O. Faergeman, J. Cohn, R. Bahr, W. Koenig, J. Demirovic, D. Arking, V. Herrera, J. Badimon, J. Goldstein, Y. Rudy, J. Airaksinen, R. Schwartz, W. Riley, R. Mendes, P. Douglas, P. Shah, From vulnerable plaque to vulnerable patient-Part III: Executive summary of the Screening for Heart Attack Prevention and Education (SHAPE) Task Force report. Am. J. Cardiol. **98**(2A), 2H–15H (2006); SHAPE Task Force Consensus Development Conference Journal Article Review United States
30. A. Nair, B. Kuban, E. Tuzcu, P. Schoenhagen, S. Nissen, D. Vince, Coronary plaque classification with intravascular ultrasound radiofrequency data analysis. Circulation **106**(17), 2200–2206 (2002)
31. A. Nair, M. Margolis, B. Kuban, D. Vince, Automated coronary plaque characterisation with intravascular ultrasound backscatter: Ex vivo validation. Eurointervention **3**(1), 113–120 (2007)
32. K. Nasu, E. Tsuchikane, O. Katoh, D. G. Vince, R. Virmani, J. F. Surmely, A. Murata, Y. Takeda, T. Ito, M. Ehara, T. Matsubara, M. Terashima, T. Suzuki, Accuracy of in vivo coronary plaque morphology assessment: A validation study of in vivo virtual histology compared with in vitro histopathology. J. Am. Coll. Cardiol. **47**(12), 2405–2412 (2006)
33. S. O'Malley, M. Naghavi, I. Kakadiaris, Image-Based Frame Gating for Stationary-Catheter IVUS Sequences. Proceedings of International Workshop on Computer Vision for Intravascular and Intracardiac Imaging, Copenhagen, Denmark, pp. 14–21, 1–6 October 2006
34. S. O'Malley, M. Vavuranakis, R. Metcalfe, C. Hartley, M. Naghavi, I. Kakadiaris, Intravascular Ultrasound-Based Imaging Of Vasa Vasorum for the Detection of Vulnerable Atherosclerotic Plaque. Proceedings of Houston Society for Engineering in Medicine and Biology, Houston, TX, 2006
35. S. O'Malley, S. Carlier, M. Naghavi, I. Kakadiaris, Image-Based Frame Gating of IVUS Pullbacks: A Surrogate for ECG. Proceedings of IEEE International Conference on Acoustics, Speech, and Signal Processing, Honolulu, HI, pp. 433–436, 15–20 April 2007
36. S.M. O'Malley, M. Naghavi, I.A. Kakadiaris, One-Class Acoustic Characterization Applied to Blood Detection in IVUS. Proceedings of 10^{th} International Conference on Medical Image Computing and Computer Assisted Intervention, Brisbane, Australia, pp. 202–209, 29 October–2 November 2007

37. S. O'Malley, J. Granada, S. Carlier, M. Naghavi, I. Kakadiaris, Image-based gating of intravascular ultrasound pullback sequences. IEEE Trans. Inform. Tech. Biomed. **12**(3), 299–306 (2008)
38. M. Papadogiorgaki, V. Mezaris, Y. Chatzizisis, G. Giannoglou, I. Kompatsiaris, Image analysis techniques for automated IVUS contour detection. Ultrasound Med. Biol. **34**(9), 1482–1498 (2008)
39. J.R. Rice, and J.S. White, Norms for smoothing and estimation, SIAM Review, 6, pp. 243–256 (1964)
40. G.A. Rodriguez-Granillo, E.P. McFadden, M. Valgimigli, C.A. van Mieghem, E. Regar, P.J. de Feyter, P.W. Serruys, Coronary plaque composition of nonculprit lesions, assessed by in vivo intracoronary ultrasound radio frequency data analysis, is related to clinical presentation. Am. Heart J. **151**(5), 1020–1024 (2006)
41. A. Roodaki, A. Taki, S.K. Setarehdan, N. Navab, *Modified Wavelet Transform Features for Characterizing Different Plaque Types in IVUS Images: A Feasibility Study*. Proceedings of 9^{th} International Conference on Signal Processing, Beijing, China, pp. 789–792, 26–29 October 2008
42. E. Sanidas, M. Vavuranakis, T. Papaioannou, I. Kakadiaris, S. Carlier, G. Syros, G. Dangas, C. Stefanadis, Study of atheromatous plaque using intravascular ultrasound. Hellenic J. Cardiol. **49**(6), 415–421 (2008)
43. K.K. Shung, M.B. Smith, B. Tsui, *Principles of Medical Imaging*. (Academic, NY, 1992)
44. A. Taki, Z. Najafi, A. Roodaki, S. Setarehdan, R. Zoroofi, A. Konig, N. Navab, Automatic segmentation of calcified plaques and vessel borders in IVUS images. Int. J. Comp. Assist. Radiol. Surg. **3**(3–4), 347–354 (2008)
45. G. Unal, S. Bucher, S. Carlier, G. Slabaugh, T. Fang, K. Tanaka, Shape-driven segmentation of the arterial wall in intravascular ultrasound images. IEEE Trans. Inform. Tech. Biomed. **12**(3), 335–347 (2008)
46. M. Vavuranakis, I.A. Kakadiaris, T.G. Papaioannou, S.M. O'Malley, S. Carlier, M. Naghavi, C. Stefanadis, Contrast-enhanced intravascular ultrasound: combining morphology with activity-based assessment of plaque vulnerability. Expert Rev. of Cardiovasc. Ther. **5**(5), 917–925 (2007)
47. M. Vavuranakis, I. Kakadiaris, S. O'Malley, C. Stefanadis, S. Vaina, M. Drakopoulou, I. Mitropoulos, S. Carlier, M. Naghavi, Detection of luminal-intima border and coronary wall enhancement in intravascular ultrasound imaging after injection of microbubbles and simultaneous sonication with transthoracic echocardiography. Circulation **112**(1), E1–E2 (2005)
48. M. Vavuranakis, T. Papaioannou, I. Kakadiaris, S. O'Malley, M. Naghavi, K. Filis, E. Sanidas, A. Papalois, I. Stamatopoulos, C. Stefanadis, Detection of perivascular blood flow in vivo by contrast-enhanced intracoronary ultrasonography and image analysis: An animal study. Clin. Exp. Pharmacol. Physiol. **34**(12), 1319–1323 (2007)
49. M. Vavuranakis, I. Kakadiaris, S. O'Malley, T. Papaioannou, E. Sanidas, M. Naghavi, S. Carlier, D. Tousoulis, C. Stefanadis, A new method for assessment of plaque vulnerability based on vasa vasorum imaging, by using contrast-enhanced intravascular ultrasound and automated differential image analysis. Int. J. Cardiol. **130**(1), 23–29 (2008)
50. D. Vince, K. Dixon, R. Cothren, J. Cornhill, Comparison of texture analysis methods for the characterization of coronary plaques in intravascular ultrasound images. Comp. Med. Imag. Graph. **24**(4), 221–229 (2000)